



ORIGINAL RESEARCH

Magnetic Fe₂O₃/biochar composite prepared in a molten salt medium for antibiotic removal in water

Huagen Liang^{1,3} · Chenxi Zhu^{1,3} · Shan Ji² · Palanisamy Kannan² · Fu Chen^{1,4}

Received: 20 July 2021 / Accepted: 28 November 2021
© The Author(s) 2022

Abstract

The large-scale use of antibiotics is causing serious water pollution problems, and it is of great significance to develop new technologies to remove antibiotics from water. As an environmentally friendly and economical adsorption material, carbon derived from biomass is a low-cost and feasible material for removing antibiotics in sewage, but the current removal efficiencies are not high enough for large-scale practical application. In this study, poplar wood chips are used as raw material, and a magnetic biochar is prepared by co-pyrolysis of poplar wood chips and FeCl₃/CaCl₂ mixed molten salt. X-ray diffraction (XRD), Fourier transform infrared spectroscopy (FTIR), N₂-isothermal adsorption and desorption, X-ray photoelectron spectroscopy (XPS) and scanning electron microscope (SEM) techniques showed the successful synthesis of Fe₂O₃/bioC composite. *In-situ* formed Fe₂O₃ makes the biochar possess the characteristic of superparamagnetic, which is conducive to the recycling of biochar. Due to the etching effect of the molten salts, rough surface was formed on Fe₂O₃/bioC, resulting in a maximum norfloxacin (NOR) adsorption ability up to 38.77 mg g⁻¹ at pH 6.0. The NOR adsorption behavior on Fe₂O₃/bioC followed the pseudo second order kinetic model and the equilibrium data was best fitted the Langmuir model. In addition, the adsorption process of NOR on Fe₂O₃/bioC was thermodynamically spontaneous. The results show that this low-cost and reusable magnetic biochar has the potential for rapid and efficient removal of antibiotic from aqueous solution.

Highlights

- A magnetic Fe₂O₃ modified porous biochar composite was prepared in a molten-salt medium.
- Molten salt made a higher proportion of micropores in Fe₂O₃/biochar during the carbonization.
- Fe₂O₃/biochars composite exhibited higher removal efficiency for NOR than original biochars.

✉ Shan Ji
jishan@zjxu.edu.cn

✉ Fu Chen
chenfu@cumt.edu.cn

¹ Jiangsu Key Laboratory of Coal-Based Greenhouse Gas Control and Utilization, Low Carbon Energy Institute, China University of Mining and Technology, Xuzhou 221008, China

² College of Biological, Chemical Science and Engineering, Jiaying University, Jiaying 314001, China

³ School of Materials Science and Engineering, China University of Mining and Technology, Xuzhou 221008, China

⁴ School of Environment Science and Spatial Informatics, China University of Mining and Technology, Xuzhou 221008, China

Keywords Antibiotic adsorption · Norfloxacin · Biochar · Water pollution · Sewage treatment

1 Introduction

Norfloxacin (NOR), a third-generation quinolone antibiotic is widely used in daily life due to its broad-spectrum antibacterial properties, low toxicity and good oral absorption (Liu et al. 2021a). In 2015, Chinese Academy of Sciences published the "Antibiotic Pollution Map of Rivers in China", showing that the average concentration of antibiotics in major rivers was about 303 ng L⁻¹, and the concentration of NOR in the Pearl River (Guangdong province) was even higher than 1000 ng L⁻¹ (Zhang et al. 2015). Antibiotics in water and soil can cause multiple threats to human body, such as toxic damage, allergic reactions, reduced immunity, and it can also lead to the evolution of drug-resistant bacteria (Luo et al. 2020; Fang et al. 2021a; Li et al. 2021). Therefore, it is of great significance to develop low-cost and highly efficient technologies to remove antibiotics from wastewater.

There are many ways to remove the antibiotics from water, such as chemical oxidation, bio-degradation, photo-degradation, electrochemical degradation, and adsorption (Langbehn et al. 2021; Wu and Hu 2021; Du et al. 2021; Hung et al. 2021; Liu et al. 2021b). Among them, the adsorption method has several advantages over other methods, including high removal efficiency, low energy consumption, easy operation, and environment-friendly. Carbon nanotubes (Ncibi and Sillanpää 2015; Soran et al. 2017), graphene (Wang et al. 2021a) and carbon aerogels (Xu et al. 2021; Liu et al. 2019a) with high specific surface area and hierarchical pore structure, are commonly used as the adsorbent. However, the complicated synthesis process and high cost of these carbon materials impede their large-scale application. Therefore, it is a promising and meaningful work to develop low-cost carbon materials with superior adsorption capability.

Currently, biochars have been developed via carbonizing the biomass and then used as electrode materials for energy storage and adsorbents for antibiotics (Rajendran et al. 2019; Zhou et al. 2021a). However, the adsorption capacities of unmodified biochars are usually quite low, and their shortcomings such as small particle size and low density are making them difficult to separate from the treated solution. Combining the magnetic medium with biomass not only enhances the adsorption performance of pollutants, but also can be easily isolated by using external magnet (Thines et al. 2017; Li et al. 2020). Shan et al. 2016 prepared magnetic Fe₃O₄/biochar by ball milling, which exhibited high removal efficiency for carbamazepine. However, the bond between Fe₃O₄ and biochar was weak, 74: which made it difficult to ensure the reusability of magnetic biochar. Fe⁰/biochar composite prepared by liquid phase reduction-deposition method almost completely adsorbed pentachlorophenol

from industrial effluent (Devi and Saroha 2014). However, nano zero valent iron was unstable in the environment, which may lead to a sharp decline in adsorption performance. Yap et al. 2017 prepared a magnetic biochar via impregnating the coconut shell with FeCl₃ and subsequent microwave pyrolysis. The results showed that the optimum adsorption capacity of magnetic biochar was achieved at the FeCl₃/biomass ratio of 0.5, due to the best pore structure. Although there are many reports on magnetic biochar, the complex synthesis methods (impregnation calcination and coprecipitation) hinder its further large-scale production. Preparing porous carbon materials in molten salt media has advantages of simple process, low synthetic temperature, easy separation, uniform chemical composition, and low cost over other methods (Pang et al. 2021; D'íez et al. 2021; Guo et al. 2020). The molten salt is a kind of ionic liquid, which can avoid the desolvation of ions in traditional chemical synthesis process, reduce activation energy, and enable rapid and efficient synthesis of materials (Huang et al. 2020). By adjusting the ratio of the mixed molten salt, the pore structure of the obtained carbon materials can be controlled precisely (Pang et al. 2021; D'íez et al. 2021). In addition, the high-energy ions in the molten state have certain etching effect, as well as recrystallization and embedding effect in the cooling stage, resulting in the formation of a hierarchical porous structure including micro-, meso-, and macro-pores in the obtained carbon material (Tan et al. 2021; Yang et al. 2020).

In this study, a magnetic Fe₂O₃/biochar composite derived from poplar wood was synthesized in mixed molten salt of CaCl₂/FeCl₃ at high temperature and then used as highly efficient adsorbent to remove NOR from water. The physical and chemical properties of biochars in the molten salt medium were investigated by XRD, TEM, and BET. The adsorption properties of the obtained magnetic biochar for NOR under different reaction conditions were evaluated, and the adsorption fitted isotherm and kinetics were also applied to study the adsorption properties. The recyclability and reuse of the as-synthesized adsorbent for NOR in water were also investigated in this study. The adsorption capability under various conditions, such as different pH, was also investigated. Also this work explored the model of adsorption isotherms and kinetics, and the adsorption mechanism of NOR.

2 Experiment

2.1 Materials and chemicals

Poplar wood (PW) was collected from local wood processing plants and further crushed and passed through a 100-mesh

sieve. Anhydrous FeCl_3 , CaCl_2 and HNO_3 were purchased from Sinopharm Chemical Reagent Co., Ltd. All the reagents were of analytical grade and used without further purification. NOR (98%) was obtained from Macklin Reagent Co., Ltd. The physicochemical properties of NOR are shown in Table 1.

2.2 Preparation of magnetic Fe_2O_3 /biochar composite

The PW sawdust was washed thoroughly with deionized water, dried and stored in an oven at 60 °C. Clean PW chips were mixed with $\text{CaCl}_2/\text{FeCl}_3$ (molar ratio = 1:2) and the ratio of PW/salts was 1:10. The mixture was put in a crucible and placed in a tubular furnace. The sample was heated up to 700–900 °C with a heating ramp of 5 °C min^{-1} in Ar atmosphere and kept at this temperature for 1 h. The sample was taken out after cooling, washed with 0.1 M HNO_3 aqueous solution (10 mL) and deionized water, filtered out and dried in a vacuum oven. The obtained carbonized sample was labeled as CPW-T, in which T stands for calcination temperature. To investigate the effect of molten salt medium, the carbonized PW sample was also prepared without adding any salt under identical conditions. The final product was denoted as PWC-T.

2.3 Physical characterizations

The obtained biochar was mixed with deionized water (mass ratio of water and biochar was 20:1), and pH of the solution was measured using pH meter (PHSJ-4F, INESA, China). The specific surface area and pore size distribution were investigated by N_2 -isothermal adsorption and desorption (Autosorb iQ, Quantachrome, USA). The vibrating sample magnetometer (PPMS-9 T, 7410 QuantunDesign, USA) was used to measure the magnetic properties of the sample. The X-ray diffraction (XRD) patterns were recorded on Shimadzu XD-3A instrument using filtered Cu-K_α radiation ($\lambda = 0.15418$ nm) at 40 kV and 30 mA. Field emission scanning electron microscope/energy-dispersive X-ray spectroscopy (SEM-EDX) (FEI QuantaTM 250, FEI, USA) was applied to observe the morphology and surface element distribution. The surface properties of biochars were

characterized by Fourier transform infrared spectroscopy (FTIR) (VERTEX 80 V, Bruker, Germany). X-ray photoelectron spectroscopy (XPS) (ESCALAB 250Xi, Thermo Fisher, USA) was used to characterize the chemical state of biochars, and the binding energy was calibrated by C_{1s} at 284.8 eV. Thermogravimetric analysis (TGA) was carried out on a TG analyzer (SDT Q600, TA, USA) at a heat rate of 10 °C min^{-1} between 25 °C and 800 °C in air.

2.4 Adsorption experiments

The stock solution of NOR (200 mg L^{-1}) was prepared by mixing NOR powder with deionized water. Prior to the tests, the stock solution was diluted to a desired concentration to form working solution. All adsorption experimental solutions were shaken at 200 rpm min^{-1} in dark box. The initial solution pH was adjusted by 0.01 mol L^{-1} HCl and 0.01 mol L^{-1} NaOH solutions. The adsorption isotherm experiments were carried out by vigorously shaking 20 mL of NOR solution (5 to 200 mg L^{-1} , pH 6) mixed with 10 mg biochar for 24 h to reach equilibrium. The adsorption kinetics was investigated by adding 10 mg of biochar into 20 mL NOR solution (50 mg L^{-1} , pH = 6). The supernatant was filtrated via centrifuging and the concentrations of NOR were measured by UV-vis spectrophotometer (UV-5500PC, Metash, China) at the wavelength of 273.0 nm. The used adsorbent was washed to neutral by deionized water and ethanol and then dried at 60 °C for the cycle test. All the experiments were performed under identical conditions.

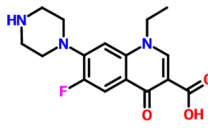
Adsorption capacity and removal efficiency were calculated by the following Eqs. (1, 2) (Kumpanenko et al. 2019):

$$q_e = \frac{(C_0 - C_e) \times V}{m} \quad (1)$$

$$R = \frac{C_0 - C_e}{C_0} \times 100\% \quad (2)$$

where, q_e is the equilibrium adsorption capacity of the corresponding biochar when the adsorption reaches equilibrium (mg g^{-1}), R is the removal efficiency (%), C_0 is the initial concentration of NOR (mg L^{-1}), C_e is the concentration

Table 1 The physical and chemical properties of NOR

Antibiotic	Formula	Molecular weight (g/mol)	Aqueous solubility (g/L, 25 °C, pH=7)	$\lg K_{ow}$ (Wang et al. 2021b)	$\text{p}K_a$ (Chen and Wang 2020)	Molecular structure
NOR	$\text{C}_{16}\text{H}_{18}\text{FN}_3\text{O}_3$	319.33	0.4	2.21	6.30/8.38	

of NOR when the adsorption reaches equilibrium (mg L^{-1}), V is the volume of the solution participating in the adsorption reaction (L), and m is the mass of added biochar (g).

3 Results and discussion

3.1 The physical and chemical properties of the obtained biochars

The material composition and crystal structure of CPW-700 and PWC-700 were firstly characterized by XRD, shown in Fig. 1a. In the XRD pattern of PWC-700, there were only 26.5° and 42.2° diffraction peaks, which corresponded to (002) and (100) crystal planes of graphitic carbon, respectively, indicating that carbon material was obtained after PW was pyrolyzed at high temperature in air. In the case of CPW-700, there were not only broad diffraction peaks around 26° , but also characteristic peaks at 24.1° , 33.2° , 40.8° , 49.5° , 54.1° , 57.6° , 62.4° , 64.0° and 71.9° were observed, corresponding to (012), (104), (113), (024), (116), (214), (300) and (1010) crystal planes of $\alpha\text{-Fe}_2\text{O}_3$ (JCPDF#33-0664) respectively. Further, the diffraction peaks at 30.3° , 35.7° , 43.3° and 63° corresponding to (206), (119), (0012) and (4012) crystal planes of $\gamma\text{-Fe}_2\text{O}_3$ (JCPDF#25-1402) respectively were also observed in the XRD pattern of CPW-700. The results showed that PW was carbonized in the molten salt media and Fe_2O_3 was formed in situ during the pyrolysis process.

Figure 1b shows the hysteresis curve measured using vibrating sample magnetometer in room temperature. It can be seen that the specific saturation magnetization of CPW-700 is 47.0 emu g^{-1} , the remanence magnetization M_r is 6 emu g^{-1} , and the coercivity H_c is 180 Oe , indicating its typical superparamagnetic behavior. The specific saturation magnetization of PWC-700 is zero, suggesting that it does not have magnetism. CPW-700 has good magnetic properties, which facilitates the separation from aqueous solution.

The porosity of CPW-700 and PWC-700 was evaluated by N_2 adsorption/desorption isotherms. As shown in Fig. 1c, there was an obvious uptake at relatively low-pressure region for both samples, implying that there were plenty of micropores in both samples. A hysteresis loop was exhibited at the relative high-pressure region of the curve of CPW-700, indicating mesopores existed in CPW-700 (Mercy et al. 2012). The hierarchical porous structure of CPW-700 was further confirmed by pore size distribution (inset of Fig. 1c). Such hierarchical porous structure not only has high surface area but also provides the pathway for efficient mass transfer (Dong et al. 2021). Table S1 (Additional file 1) shows the porous parameters of two samples. The Brunauer–Emmett–Teller (BET) specific surface area of CPW-700 is $431.6 \text{ m}^2 \text{ g}^{-1}$, slightly higher than that of

PWC-700 ($422.1 \text{ m}^2 \text{ g}^{-1}$). The average pore size of CPW-700 calculated by DFT method is ca. 2.1 nm , smaller than that of PWC-700 (3.2 nm). In the molten salt system, the eutectic point of mixed molten salts of $\text{CaCl}_2/\text{FeCl}_3$ is only 100°C , when the molar ratio of CaCl_2 to FeCl_3 is 1:2 (http://www.factsage.cn/fact/documentation/FTsalt/FTsalt_list.htm). The liquid molten salt can penetrate into the pores of biomass, etching the biomass during the carbonization, forming more micropores. Simultaneously, Fe_2O_3 nanoparticles were also formed in-situ and embedded in carbon material, resulting in relatively low narrower pore sizes.

FTIR spectra of CPW-700 and PWC-700 (Fig. 1d) showed many absorption peaks, which represented different functional groups in the samples. The peaks in the 3691 , 1715 and 1140 cm^{-1} bands were caused by stretching vibrations of $-\text{OH}$, $\text{C}=\text{O}$, and $-\text{COOH}$, respectively, indicating that both samples contained abundant oxygen-containing functional groups. Peaks at $1500\text{--}1550 \text{ cm}^{-1}$ resulted from $\text{C}=\text{C}$ stretching vibration (Wu et al. 2019). For CPW-700, vibration peaks of $\text{Fe}\text{--}\text{O}$ bonds were also found at 640 , 565 and 471 cm^{-1} , which were attributed to the deformation vibration and stretching vibration of Fe_2O_3 , further confirming that Fe_2O_3 was successfully loaded on the obtained biochar (Pardeep et al. 2014). The absorption peak at 887 cm^{-1} indicates the presence of aromatic functional groups on the surface. These aromatic groups can provide electron donors, adsorb and bind NOR through the interaction between the electron donor and NOR. Therefore, it is expected that the CPW-700 with aromatic groups on the surface will exhibit a better NOR adsorption capacity.

The surface composition and chemical state of the obtained biochars were evaluated by XPS analysis. The XPS spectra of CPW-700 showed the presence of iron on its surface (Fig. 1e). The high-resolution $\text{C } 1s$ spectra were fitted into three peaks (Additional file 1: Fig. S1a). The peak at 284.8 eV corresponds to $\text{C}\text{--}\text{C}/\text{C}=\text{C}$, and the two peaks between 286 and 290 eV ascribes to oxygen-containing functional groups ($\text{C}\text{--}\text{O}/\text{C}=\text{O}$) and $\pi\text{--}\pi^*$ vibration satellite peaks respectively (Jo et al. 2020). The high-resolution $\text{Fe } 2p$ spectrum of the TMBC-700 sample (Fig. 1f) was fitted into 4 different peaks, in which the peaks at 710.9 and 724.1 eV are attributed to $\text{Fe}^{3+} 2p_{3/2}$ and $\text{Fe}^{3+} 2p_{1/2}$ orbitals, while 712.9 and 726.5 eV correspond to satellite peaks (Zhou et al. 2021b). No Fe signal was detected in the XPS of PWC-700. In the fitted $\text{O } 1s$ XPS spectrum (Additional file 1: Fig. S1b), the peaks at 530.4 and 532.6 eV in TMBC-700 corresponded to $\text{Fe}\text{--}\text{O}$ bond (Shi et al. 2021), the peak at 531.2 eV ascribed to the $-\text{OH}$ or $-\text{OOH}$ bonds (Zhang et al. 2020), and the peak at 533.0 eV resulted from the $-\text{OH}$ bond of adsorbed water molecules (Liu et al. 2019b), indicating that the Fe_2O_3 was loaded on CPW-700.

Figure 2a and c exhibit that both CPW-700 and PWC-700 remain the original honeycomb-like structure of the

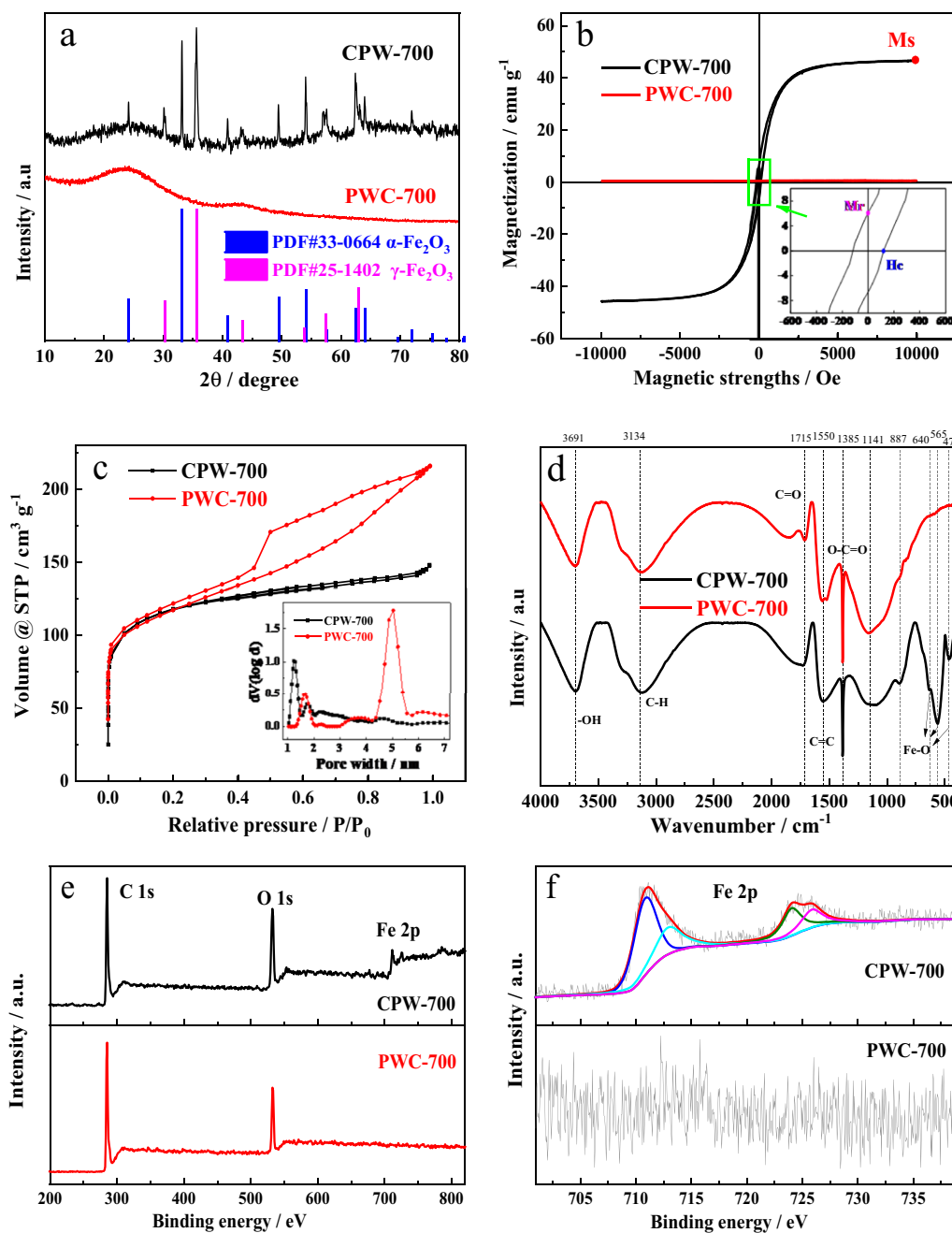


Fig. 1 XRD patterns **a**, magnetic hysteresis curves **b**, N₂ adsorption/desorption isotherms **c** and corresponding pore size distribution (inset), FTIR spectra **d**, Survey XPS spectrum **e** and high-resolution XPS spectrum of Fe 2p **f** of CPW-700 and PWC-700

PW after carbonization. As shown in Fig. 2b and d, the main difference between CPW-700 and PWC-700 is that the surface of CPW-700 is quite rough and coated with a layer similar to the accumulation of nanoparticles, while the surface of PWC-700 was very smooth. The elemental distribution of CPW-700 and PWC-700 was analyzed by

EDS. Figure S2a (Additional file 1) shows that the C, O, N and Fe elements are evenly distributed in CPW-700, while only C, O, and N elements were detected in PWC-700 (Additional file 1: Fig. S2b), which further implied that the Fe₂O₃ was evenly distributed in CPW-700.

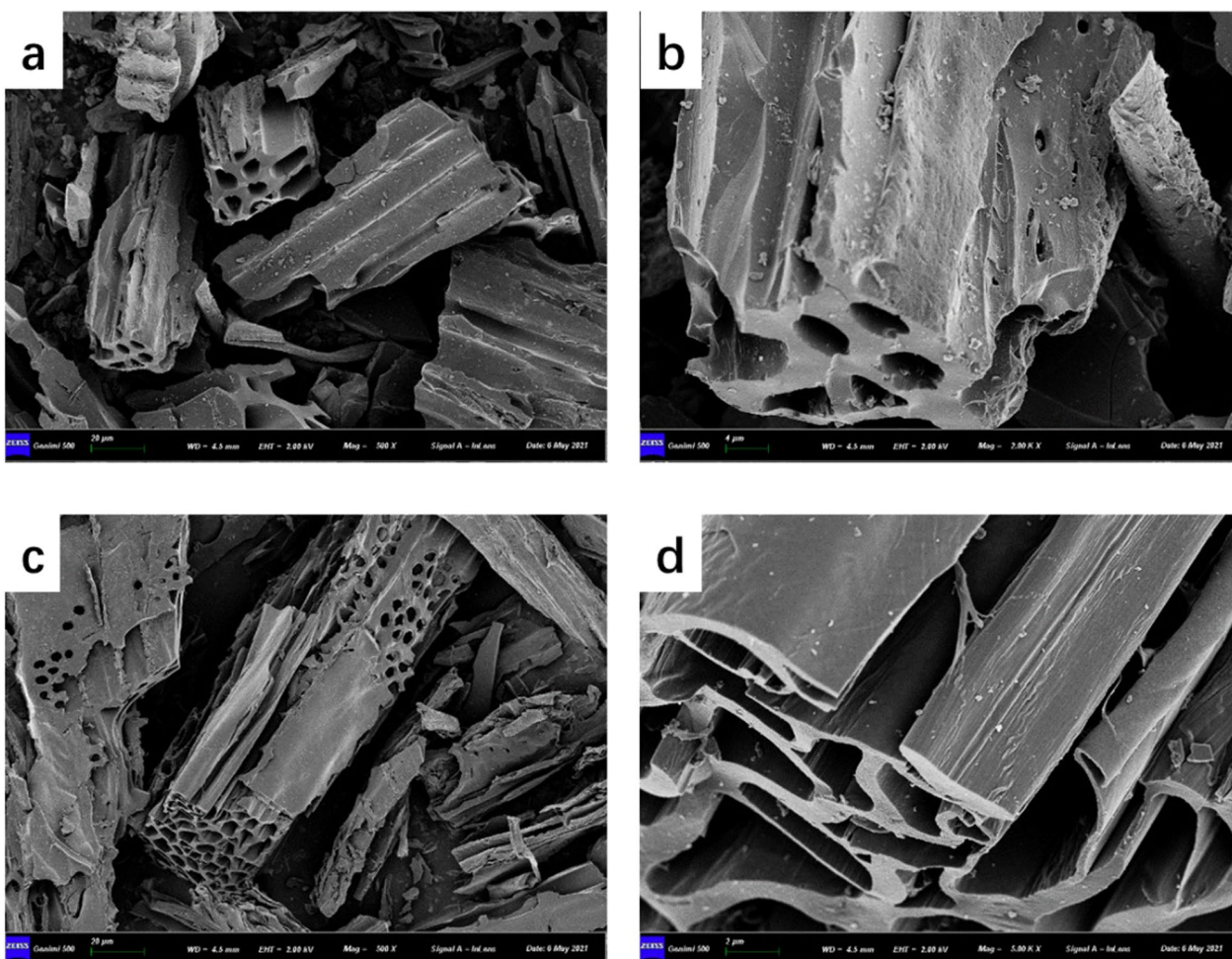


Fig. 2 SEM images of CPW-700 a, b and PWC-700 (c, d)

3.2 Adsorption capability

3.2.1 The effect of carbonizing temperature on the adsorption performance of NOR

Under the fixed ratio of molten salt and PW, the effect of carbonizing temperature on the adsorption of NOR was investigated. As shown in Fig. 3, when the dosage of biochar was 1 g L^{-1} , as the carbonizing temperature increased, the removal efficiency of NOR by biochar showed an upward trend, which could result from the moisture. Notably, volatile substance of biomass gradually escaped with the increase of the temperature, forming plenty of porous structures in the biochars. Compared with PWC-700, there is a significant enhancement of the removal rate of NOR for CPW-700 (Ge et al. 2021). Due to the etching effect of the molten salts, rough surface was formed on CPW-700, which could provide more adsorbing sites for NOR. The BET results showed that the specific surface of CPW-700 was higher than that of

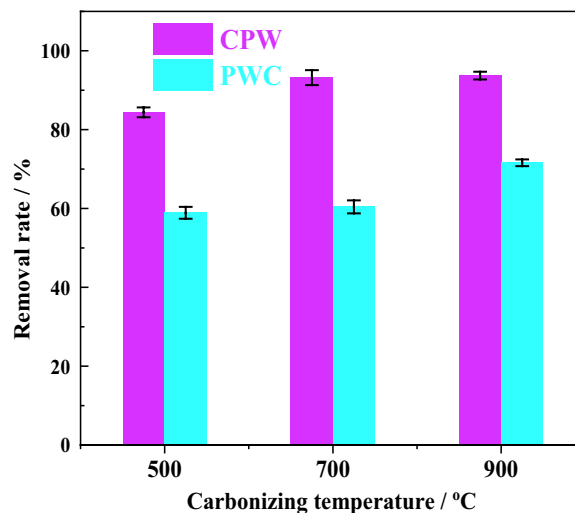


Fig. 3 The effect of carbonizing temperature of biochar on adsorption performance for NOR. Error bars represent the standard deviation of four measurements

PWC-700, especially there was a higher micropore ratio in CPW-700, which can facilitate the mass transfer, resulting in a better adsorption capability of NOR.

3.2.2 The effect of pH and biochar dosage on the adsorption capability of NOR

Antibiotics are usually polar and hydrophobic materials, and thus electrostatic attraction, hydrophobic distribution, π - π conjugation, cation exchange, and hydrogen bonding may be involved in the mechanism of their adsorption. The pH value of NOR solution may affect the surface charge of the biochar. In addition, NOR has two acid dissociation constants in aqueous solution, $pK_{a1} = 6.30$ (related to the deprotonation of the carboxyl group (-COOH)) and $pK_{a2} = 8.38$ (related to the protonation of the amino group (-N₂C₄H₉) on the piperazinyl group). Therefore, At $pH \leq 6.34$, NOR 6.34, NOR molecules are mainly present in cationic form (NOR⁺); at $pH > 8.75$, NOR molecules are mainly present as NOR⁻ in solution; Proton dissociation occurs and NOR mainly exist in the form of neutral molecules or amphoteric NOR. pH value is directly related to the existed form of NOR molecules (Fu et al. 2021).

Therefore, the NOR adsorption ability of CPW-700 was investigated in the pH range of 3.0–9.0, as shown in Fig. 4a. When the dosage of CPW-700 was 0.5 g L⁻¹ and the initial concentration of NOR was 20 mg L⁻¹, the removal efficiency of NOR first increased and then decreased as the pH increased, and reached the maximum value of 38.77 mg g⁻¹ at pH 6. When the pH is low, the protonation of the biochar surface makes it have a large amount of positive charge, and the electrostatic repulsion between H⁺ and NOR⁺ is inevitable. The plenty of surface adsorption sites are occupied by H⁺, so the adsorption capability of NOR is low in the strong acid condition. As the pH value increases, the adsorption of H⁺ on biochar decreases, resulting in more NOR⁺ adsorbs on biochar. Under alkaline conditions, the NOR⁻ in the solution increases with the pH. In such solution, the hydrogen bonding and cation exchange are inhibited, and there is also the repulsion of OH⁻ and NOR⁻, which leads to the decline of NOR adsorption (Gege et al. 2018).

It was clear that, the maximum adsorption capacity of CPW-700 for NOR was 38.77 mg g⁻¹ when the pH value was 6. Compared with other biochars, the adsorption performance of CPW-700 was competitive, as shown in Table 2.

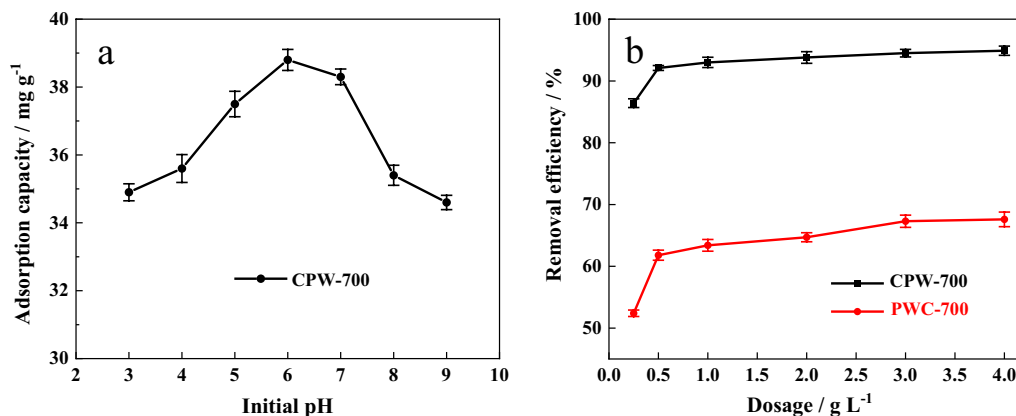


Fig. 4 The effect of pH a and biochar dosage b on NOR adsorption. Error bars represent the standard deviation of four measurements

Table 2 The adsorption performances of different biochar

Adsorbents	Antibiotics	Adsorption uptake (mg g ⁻¹)	Reference
Iron ore wastes	Norfloxacin	8.64	Fang et al. 2021b)
Fe/Zn/H ₃ PO ₄ /sludge biochar	Norfloxacin	39.3	Ma et al. 2020)
Clay-biochar	Norfloxacin	3.86	Li et al. 2017)
γ -Fe ₂ O ₃ /biochar	Norfloxacin	7.62	Wang et al. 2017)
Carbonated cauliflower root	Norfloxacin	4.13	Qin et al. 2017)
Rice husk ash	Tetracycline	8.37	Chen et al. 2016)
Iron ore/biochar	Norfloxacin	2.45	Yang et al. 2019)
γ -Fe ₂ O ₃ @biochar	Norfloxacin	5.52	Wang et al. 2020)
Fe ₂ O ₃ /biochar	Norfloxacin	38.77	This work

The effect of biochar dosage on the percent removal of the studied antibiotic is depicted in Fig. 4b in the range of 0.25–4.0 g L⁻¹. As the dosage increased from 0.25 to 0.5 g L⁻¹, the removal efficiency of antibiotics increased. After the dosage of CPW-700 or PWC-700 increased more than 1.0 g L⁻¹, the change of adsorption efficiency for NOR was not obvious. The changing trend of removal efficiency could be due to the increased dosage of biochar providing more active adsorption sites and functional groups, resulting in stronger interaction between biochar and antibiotics. However, when too much adsorbent was used, the adsorption and desorption of antibiotics reached a balance, and the removal efficiency almost did not increase (Amin et al. 2017). Compared with CPW-700, despite the continuous increase in the dosage, the NOR adsorption of PWC-700 did not exceed 70%. These results demonstrated that the FeO₃ had a significantly positive effect on NOR adsorption. 0.5 g L⁻¹ of dosage was selected for subsequent experiments.

3.2.3 Adsorption kinetic studies

The adsorption kinetic equation can reflect the reaction pathways and adsorption mechanism (Plazinski et al. 2009). As shown in Fig. 5a, the NOR adsorption capacity increased with the adsorption time on both samples. At the initial stage (the first 30 min), the adsorption rate of both samples was quite high. After that, the adsorption rate rapidly decreased and quickly reached adsorption equilibrium. In the beginning, there are plenty of adsorption sites available on these samples for NOR, so the adsorption rate is quite high. As the time increases, the effective adsorption sites on the sample surface gradually decrease. NOR needs to diffuse into the micropores to reach the adsorption sites, causing adsorption rate to slow down, and finally, the adsorption reaches a dynamic equilibrium (Lyu et al. 2017; Mohan et al. 2007).

In this study, the commonly used pseudo-first-order, pseudo-second-order kinetics, and intra-particle diffusion

model equations were used to fit the adsorption data (Garzo et al. 2021).

Pseudo-first order dynamics model, as Eq. (3):

$$\ln\left(1 - \frac{q_t}{q_e}\right) = -k_1 t \quad (3)$$

Pseudo-second order dynamics model, as Eq. (4):

$$\frac{t}{q_t} = \frac{1}{k_2 q_e^2} + \frac{t}{q_e} \quad (4)$$

Intra-particle diffusion model, as Eq. (5):

$$q_t = k_3 \sqrt{t} + c \quad (5)$$

in which t is the adsorption time (min), q_e is the equilibrium adsorption capacity of biochar when the adsorption reaches equilibrium (mg/g), q_t is the adsorption capacity of biochar corresponding to time (mg/g); k_1 is the rate constant of the quasi-first order kinetic equation (min⁻¹), k_2 is the rate constant of the quasi-second order kinetic equation (g/mg/min), k_3 is the diffusion constant (g/mg/min^{1/2}), and c is the thickness constant of the interface layer.

Table S2 (Additional file 1) shows that the correlation coefficients fitted by the pseudo-second-order kinetic equations ($R_2 = 0.9991, 0.9977$) are all larger than those fitted by the pseudo-first-order kinetic equations (0.9936, 0.9041) and the intra-particle diffusion model equations (0.6136, 0.5863), and the fitted adsorption value is closer to the actual, indicating that the pseudo-second-order kinetics fits the NOR adsorption data more closely. The adsorption rate of biochar is mainly determined by chemical adsorption mechanism. NOR is mainly adsorbed on the surface of biochar via interacting with the π - π electron acceptor/donor, electrostatic attraction, and hydrogen bonding. It is a result of the combined effect of the above various influencing factors (Tan et al. 2008). Figure 5b shows that the

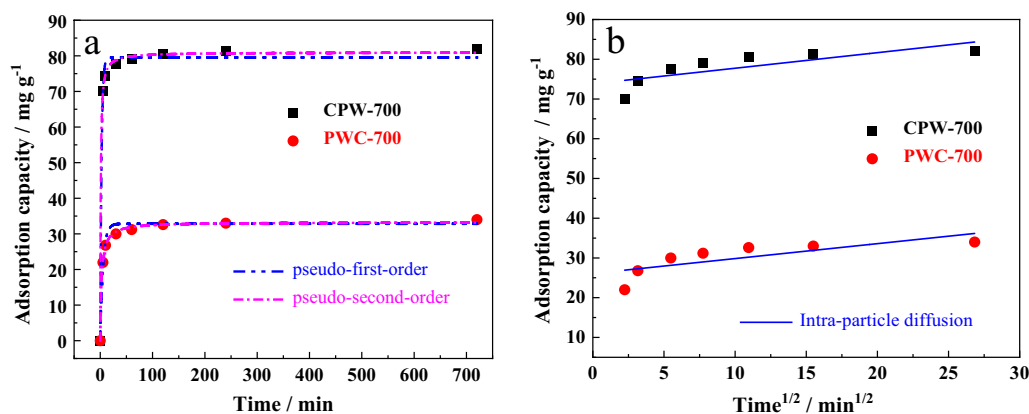


Fig. 5 Adsorption kinetics **a** and intra-particle diffusion model **b** for NOR adsorption on CPW-700 and PWC-700

fitting straight line of the intra-particle diffusion model does not pass the coordinate origin, and the c value is not zero, showing that the intra-particle diffusion is not the only rate-determining step in the adsorption process. A linear fitting was performed on the latter stage of the model, and it was found that the diffusion constants ki were not much different, indicating that the boundary layer effect and mass transfer resistance of the diffusion increased to the peak value, and then gradually reached a balance (Zhou et al. 2017).

3.2.4 Equilibrium isotherm studies

The adsorption isotherm can reflect the affinity of the adsorbent to the adsorbate and describe the interaction between the adsorbate and the adsorbent (Xia et al. 2019). The adsorption isotherms of biochar in NOR solutions with different initial concentrations at 25 °C are shown in Fig. 6. Langmuir and Freundlich isotherm adsorption models were used to simulate the NOR adsorption performance of the two samples (Leandro-Silva et al. 2020). Their equations can be expressed as follows:

Freundlich isotherm model, as Eq. (6):

$$Q_e = K_f C_e^{1/n} \tag{6}$$

Langmuir isotherm model, as Eq. (7):

$$Q_e = \frac{Q_m K_L C_e}{1 + K_L C_e} \tag{7}$$

In Freundlich isotherm model, Q_e represents the equilibrium adsorption capacity (mg g^{-1}), C_e represents the concentration of adsorbate when the adsorption reaches equilibrium (mg L^{-1}), K_f represents the Freundlich affinity coefficient ($\text{mg}^{1-n} \text{g}^{-1} \text{L}^{-n}$), n denotes an empirical parameter of adsorption strength.

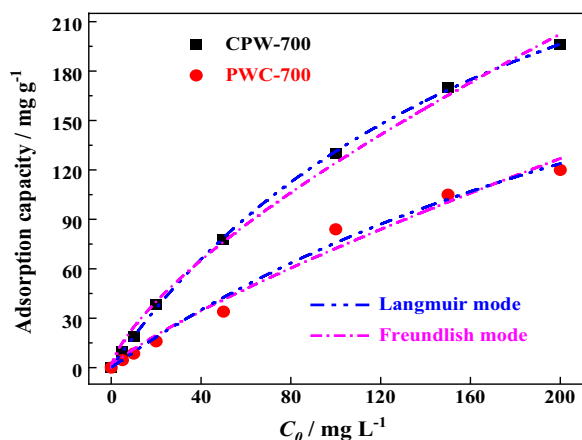


Fig. 6 Adsorption isotherms of NOR on CPW-700 and PWC-700

In Langmuir isotherm model, Q_m (mg g^{-1}) is the maximum adsorption capacity, and K_L (mg L^{-1}) is the Langmuir adsorption constant.

The adsorption rates of both CPW-700 and PWC-700 increased with the initial concentration of NOR, and the NOR adsorption amount rate on CPW-700 was higher than that on PWC-700. From the shape of the isotherm, the two samples are in line with the Freundlich and Langmuir isotherms, but the Langmuir model fits better, indicating that the adsorption of NOR on biochar is a single-layer adsorption process. The maximum adsorption capacity (Q_m) calculated via the model for CPW-700 (379.85 mg g^{-1}) was higher than PWC-700 (275.69 mg g^{-1}), shown in Table S3 (Additional file 1). The value of n in the Freundlich model is related to the properties of the adsorption material and the adsorption system. Generally, the value of n indicates the difficulty rate of adsorption process, in other words, the smaller $1/n$ value represents the easy adsorption process. The $1/n$ value of CPW-700 is smaller than that of PWC-700, indicating that NOR adsorption is easier to occur on CPW-700 (Ding et al. 2013).

3.2.5 Adsorption thermodynamics

Thermodynamic study was used to describe the driving force and to estimate whether the process of the adsorption of NOR onto biochars was spontaneous or not. The equations are as follows:

$$\Delta G = -RT \ln K_d \tag{8}$$

$$\Delta G = \Delta H - T \Delta S \tag{9}$$

$$\ln K_d = -\Delta H/RT + \Delta S/R \tag{10}$$

where ΔG is the Gibbs free energy change (kJ mol^{-1}), ΔH is the enthalpy change (kJ mol^{-1}), ΔS is the entropy change ($\text{J mol}^{-1} \text{K}^{-1}$), T is the absolute temperature (K) and R is the universal gas constant ($8.314 \text{ J mol}^{-1} \text{K}^{-1}$); K_d is the equilibrium distribution coefficient, which is the ratio of the amount adsorbed on the adsorbents (mg g^{-1}) to the equilibrium concentration in solution (mg L^{-1}).

The thermodynamic parameters of CPW-700 and PWC-700 for the NOR adsorption process are shown in Table S4 (Additional file 1), according to Van't Hoff equation (see supporting information). Through calculating the data at three different temperatures, it was found that the obtained ΔG was less than 0, indicating that the adsorption process was spontaneous, and the absolute value of ΔG increased with the temperature, showing that the temperature promoted the spontaneous NOR adsorption. The obtained ΔH of both samples was greater than zero, indicating that the NOR adsorption process was endothermic, so heating up

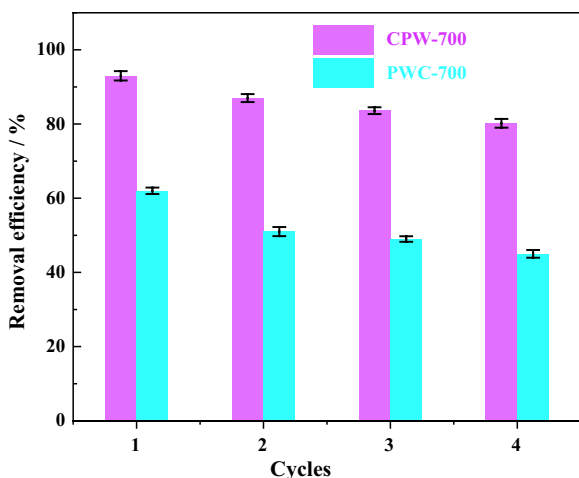


Fig. 7 The reusability of CPW-700 and PWC-700. Error bars represent the standard deviation of four measurements

was beneficial to adsorption, which was also consistent with the results of isotherm adsorption. The entropy changes ΔS of CPW-700 and PWC-700 were positive values of 0.0567 and 0.0198 $\text{kJ mol}^{-1} \text{K}^{-1}$. The positive ΔS values of both samples indicate that the adsorption process favors sorption stability (Xia et al. 2019; Wang et al. 2018).

3.2.6 Adsorption reusability

As well known, the reusability of adsorbent is very important in practical application. After each run, the biochar was collected, washed by distilled water and ethanol for three times, and dried in vacuum oven at 60 °C for 6 h. Subsequently, the clean biochar after each adsorption experiment was remixed with NOR solution. As shown in Fig. 7, the removal efficiencies of CPW-700 and PWC-700 in the second time were 87.06 and 51.44%, dropping to 83.62% and 49.32% in the third time, and 80.21% and 45.07% in the fourth time, respectively. Although the removal efficiency of both samples decreased, the removal efficiency of CPW-700 was still considerable, higher than 80%, much higher than that of PWC-700. Thus, CPW-700 had a better reusability than PWC-700.

3.2.7 NOR adsorption mechanism

In order to explore the adsorption mechanism of biochars for NOR, the FTIR and N_2 isothermal adsorption desorption curves before and after adsorption were investigated. As shown in Fig. S3 (Additional file 1), it was clear that some changes took place in the characteristic peaks of FTIR before and after adsorption. The stretching vibration peaks at 1562 cm^{-1} , 640 cm^{-1} , 565 cm^{-1} and 471 cm^{-1} shifted slightly after adsorption. It can be inferred that

the corresponding functional groups were involved in the adsorption reaction of NOR. The weakening of -OH characteristic peak intensity proves the importance of hydrogen bonding in the reaction process. Solis et al. (Solis et al. 2021) confirmed that hydrogen bonds can promote the adsorption of polar organic compounds on biochar. -COOH, -OH and other oxygen-containing functional groups can interact with O, N, and F atoms in NOR molecule in the form of hydrogen bonds. The shift of C=C and the weakening of peak intensity of O-C=O show that π - π interaction plays a role in the adsorption process of composites and NOR. Due to the presence of strong electron-attracting element F in the NOR, the electron density on the benzene ring was reduced, as a π -electron acceptor, while the aromatic functional group on the surface of the biochar can be used as a π -electron donor to form π - π electron donor-acceptor interaction of NOR, which could be another adsorption effect between NOR and biochar (Wang et al. 2010). At the same time, the peak position of Fe-O stretching vibration peak also shifted to a certain extent, indicating that Fe-O may provide more adsorption sites for the adsorption of NOR.

From Fig. S4 (Additional file 1), it can be seen that the volume of CPW-700 and PWC-700 after adsorbing NOR decreases significantly. In addition, the pore size distribution also changed significantly (as shown in the illustration of Fig. S4 (Additional file 1)). Only mesopores of 3.7 nm existed in PWC-700, while 2–8 nm mesopores can hardly be detected in CPW-700. Moreover, BET specific surface area, average pore diameter and pore volume of CPW-700 and PWC-700 after adsorbing NOR decreased (Additional file 1: Table S5), implying that pore filling may be one of the forces for biochar adsorbing NOR. Chun et al. (Chun et al. 2004) suggested that the specific surface area and pore structure are important factors that affect the adsorption of organic pollutants by biochar, and the organic pollutants are adsorbed on the biochar through pore-filling mechanism. It is clear to see from the Fig. 4a that the adsorption efficiency of NOR on CPW-700 is the

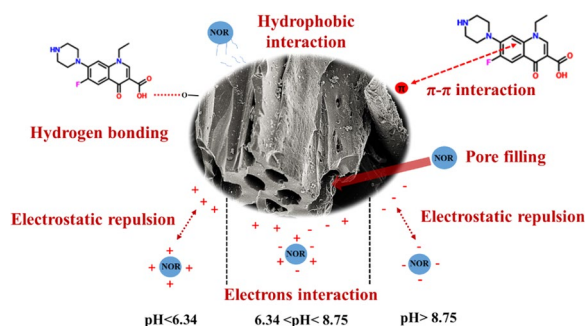


Fig. 8 Schematic diagram of NOR adsorption mechanisms on CPW-700

highest when the pH value is close to neutral, indicating that hydrophobicity is the main force between CPW-700 and NOR. Therefore, as shown in Fig. 8, we believe that the adsorption process of biochar and NOR molecules may be a synergistic effect of hydrogen bonding, π - π electron donor and acceptor interaction, and pore filling.

4 Conclusions

Fe₂O₃ nanoparticles modified magnetic porous biochar derived from PW was prepared in a molten-salt medium. The obtained CPW-700 exhibited a superior NOR adsorption capability due to high surface area, pore volume, and the presence of functional groups on the surface. The obtained biochar followed the pseudo-second-order kinetic model, and the main forms of adsorption could be liquid film diffusion and surface adsorption. The adsorption isotherm data of CPW-700 is more in line with the Langmuir model. The adsorption process of NOR on CPW-700 is determined by multiple factors, including pore filling, hydrogen bonding, π - π electron donor-acceptor interaction, electrostatic repulsion, and hydrophobic interaction. The results show that magnetic porous biochar developed in this study is a promising feasible adsorbent for removing antibiotics from water.

Supplementary Information The online version contains supplementary material available at <https://doi.org/10.1007/s42773-021-00130-1>.

Acknowledgements The Key Laboratory of Fuel Cell Technology of Guangdong Province provided the funding for this research.

Authors' contributions HL: Conceptualization, Methodology, Investigation, Validation, Formal analysis, Visualization, Resources, Data curation, Writing-original draft, Supervision, Project administration, Funding acquisition. CZ: Conducting a research and investigation process, specifically performing the experiments, or data/evidence collection. SJ: Writing-review & editing. PK: Investigation, Writing-review & editing. FC: Supervision, Project administration, Funding acquisition.

Funding National Natural Science Foundation of China, Grant Number: 21908242.

Data availability The datasets used or analysed during the current study are available from the corresponding author on reasonable request.

Declarations

Conflict of interest The authors declare no conflicts of interest.

Open Access This article is licensed under a Creative Commons Attribution 4.0 International License, which permits use, sharing, adaptation, distribution and reproduction in any medium or format, as long as you give appropriate credit to the original author(s) and the source, provide a link to the Creative Commons licence, and indicate if changes were made. The images or other third party material in this article are

included in the article's Creative Commons licence, unless indicated otherwise in a credit line to the material. If material is not included in the article's Creative Commons licence and your intended use is not permitted by statutory regulation or exceeds the permitted use, you will need to obtain permission directly from the copyright holder. To view a copy of this licence, visit <http://creativecommons.org/licenses/by/4.0/>.

References

- Amin MT, Alazba AA, Shafiq M (2017) Removal of copper and lead using banana biochar in batch adsorption systems: isotherms and kinetic studies. *Arab J Sci Eng* 43:5711–5722
- Chen X, Wang J (2020) Degradation of norfloxacin in aqueous solution by ionizing irradiation: Kinetics, pathway and biological toxicity. *Chem Eng J* 395:125095
- Chen Y, Wang F, Duan L, Yang H, Gao J (2016) Tetracycline adsorption onto rice husk ash, an agricultural waste: Its kinetic and thermodynamic studies. *J Mol Liq* 222:487–494
- Chun Y, Sheng G, Chiou CT, Xing B (2004) Compositions and sorptive properties of crop residue-derived chars. *Environ Sci Technol* 38:4649–4655
- D'iez N, Fuertes AB, Sevilla M (2021) Molten salt strategies towards carbon materials for energy storage and conversion. *Energy Storage Mater* 38:50–69
- Devi P, Saroha AK (2014) Synthesis of the magnetic biochar composites for use as an adsorbent for the removal of pentachlorophenol from the effluent. *Biores Technol* 169:525–531
- Ding Y, Wang D, Jing DB, Huang ZD, Wang Z (2013) Adsorption of Aquatic Cadmium (II) by Chestnut Inner Shell, 2013 Third International Conference on Intelligent System Design and Engineering Applications (Isdea), 222–226.
- Dong Q, Zhang F, Ji S, Wang X, Wang H, Linkov V, Wang R (2021) Fe₃C-inserted “tube plugging into porous network” nanohybrids as advanced sulfur hosts for lithium-sulfur batteries. *J Alloys Compd* 877:160286
- Du C, Zhang Z, Yu G, Wu H, Chen H, Zhou L, Zhang Y, Su Y, Tan S, Yang L, Song J, Wang S (2021) A review of metal organic framework (MOFs)-based materials for antibiotics removal via adsorption and photocatalysis. *Chemosphere* 272:129501
- Fang L, Miao Y, Wei D, Zhang Y, Zhou Y (2021a) Efficient removal of norfloxacin in water using magnetic molecularly imprinted polymer. *Chemosphere* 262:128032
- Fang N, He Q, Sheng L, Xi Y, Zhang L, Liu H, Cheng H (2021b) Toward broader applications of iron ore waste in pollution control: Adsorption of norfloxacin. *J Hazard Mater* 418:126273
- Fu L, Jiang L, Liao K, An J, Huang W, Sun X, Li T, He Y (2021) Adsorption behavior of welan gum on quartz sand in reservoir. *J Pet Sci Eng* 205:108850
- Garzo V, Brito R, Soto R (2021) Navier-Stokes transport coefficients for a model of a confined quasi-two-dimensional granular binary mixture. *Phys Fluids* 33:023310
- Ge X, Wu Z, Manzoli M, Bonelli B, Mantegna S, Kunz W, Cravotto G (2021) Adsorptive decontamination of antibiotic-spiked water and milk using commercial and modified activated carbons. *J Environ Chem Eng* 9:105544
- Gege W, Jiping M, Shuang L, Jing G, Bo J, Liyan W, Jinhua L, Xiaoyan W, Lingxin C (2018) Magnetic copper-based metal organic framework as an effective and recyclable adsorbent for removal of two fluoroquinolone antibiotics from aqueous solutions. *J Colloid Interface Sci* 528:360–371

- Guo Z, Kong X, Wu X, Xing W, Zhou J, Zhao Y, Zhuo S (2020) Heteroatom-doped hierarchical porous carbon via molten-salt method for supercapacitors. *Electrochim Acta* 360:137022
- Huang L, Hu Z, Jin H, Wu J, Liu K, Xu Z, Wan J, Zhou H, Duan J, Hu B, Zhou J (2020) Salt-assisted synthesis of 2D materials. *Adv Func Mater* 30:1908486
- Hung A, Yan M, Lin J, Xu L, Gong H, Gong H (2021) A review of processes for removing antibiotics from breeding wastewater. *Int J Environ Res Public Health* 18:4909
- Jo W-K, Moru S, Lee D-E, Tonda S (2020) Cobalt- and iron-coordinated graphitic carbon nitride on reduced graphene oxide: A nonprecious bimetallic M-N_x-C analogue electrocatalyst for efficient oxygen reduction reaction in acidic media. *Appl Surf Sci* 531:147367
- Kumpanenko IV, Ivanova NA, Dyubyanov MV, Skryl'nikov AM, Koval'eva NY, Roshchin AV (2019) Removal of Mercury(II) from aqueous solutions via dynamic column adsorption. *Russ J Phys Chem B* 13:502–513
- Langbehn RK, Michels C, Soares HM (2021) Antibiotics in wastewater: From its occurrence to the biological removal by environmentally conscious technologies. *Environ Pollut* 275:116603
- Leandro-Silva E, Pippi ARF, Magdalena AG, Piacenti-Silva M (2020) Application of Langmuir and Freundlich models in the study of banana peel as bioadsorbent of copper (II) in aqueous medium. *Materia-Brazil* 25:e12656
- Li Y, Wang Z, Xie X, Zhu J, Li R, Qin T (2017) Removal of Norfloxacin from aqueous solution by clay-biochar composite prepared from potato stem and natural attapulgite. *Colloids Surf A* 514:126–136
- Li X, Wang C, Zhang J, Liu J, Liu B, Chen G (2020) Preparation and application of magnetic biochar in water treatment: A critical review. *Sci Total Environ* 711:134847
- Li N, He M, Lu X, Liang L, Li R, Yan B, Chen G (2021) Enhanced norfloxacin degradation by visible-light-driven Mn₃O₄/γ-MnOOH photocatalysis under weak magnetic field. *Sci Total Environ* 761:143268
- Liu H, Wei Y, Luo J, Li T, Wang D, Luo S, Crittenden JC (2019a) 3D hierarchical porous-structured biochar aerogel for rapid and efficient phenolic antibiotics removal from water. *Chem Eng J* 368:639–648
- Liu Y, Hu Y, Ma P, Li F, Yuan F, Wang S, Luo Y, Ma J (2019b) Amorphous CoFe double hydroxides decorated with N-Doped CNTs for efficient electrochemical oxygen evolution. *Chemosuschem* 12:2679–2688
- Liu Y, Chen Y, Feng M, Chen J, Shen W, Zhang S (2021a) Occurrence of antibiotics and antibiotic resistance genes and their correlations in river-type drinking water source, China. *Environ Sci Pollut Res* 28:42339–42352
- Liu P, Wu Z, Abramova AV, Cravotto G (2021b) Sonochemical processes for the degradation of antibiotics in aqueous solutions: a review. *Ultrason Sonochem* 74:105566–105566
- Luo Y, Huang X, Li Y, Fu Y, Wang Z, Lu J, Zhang J (2020) CuNiN@C coupled with peroxydisulfate as efficient catalytic system for the removal of norfloxacin by adsorption and catalysis. *Sep Purif Technol* 252:117476
- Lyu H, Tang J, Huang Y, Gai L, Zeng EY, Liber K, Gong Y (2017) Removal of hexavalent chromium from aqueous solutions by a novel biochar supported nanoscale iron sulfide composite. *Chem Eng J* 322:516–524
- Ma Y, Li P, Yang L, Wu L, He L, Gao F, Qi X, Zhang Z (2020) Iron/zinc and phosphoric acid modified sludge biochar as an efficient adsorbent for fluoroquinolones antibiotics removal. *Ecotoxicol EnviRon Saf* 196:110550
- Mercy RB, Gurudas PM, Siddulu NT, Shaji V, Chokkalingam A, Salem SA, Veerappan VB, Ajayan V (2012) Microwave-assisted synthesis of highly crystalline mesoporous hydroxyapatite with a rod-shaped morphology. *Chem Soc Jpn* 41:458–460
- Mohan D, Pittman CU Jr, Bricka M, Smith F, Yancey B, Mohammad J, Steele PH, Alexandre-Franco MF, Gómez-Serrano V, Gong H (2007) Sorption of arsenic, cadmium, and lead by chars produced from fast pyrolysis of wood and bark during bio-oil production. *J Colloid Interface Sci* 310:57–73
- Ncibi MC, Sillanpää M (2015) Optimized removal of antibiotic drugs from aqueous solutions using single, double and multi-walled carbon nanotubes. *J Hazard Mater* 298:102–110
- Pang Z, Li G, Xiong X, Ji L, Xu Q, Zou X, Lu X (2021) Molten salt synthesis of porous carbon and its application in supercapacitors: a review. *J Energy Chem* 61:622–640
- Pardeep S, Pankaj R, Shailza K, Amit K, Deepak P, Pankaj T (2014) Solar-Fenton removal of malachite green with novel Fe⁰-activated carbon nanocomposite. *Appl Catal A* 476:9–18
- Plazinski W, Rudzinski W, Plazinska A (2009) Theoretical models of sorption kinetics including a surface reaction mechanism: a review. *Adv Coll Interface Sci* 152:2–13
- Qin T, Wang Z, Xie X, Xie C, Zhu J, Li Y (2017) A novel biochar derived from cauliflower (*Brassica oleracea* L.) roots could remove norfloxacin and chlortetracycline efficiently. *Water Sci Technol* 76:3307–3318
- Rajendran M, Shi L, Wu C, Li W, An W, Liu Z, Xue S (2019) Effect of sulfur and sulfur-iron modified biochar on cadmium availability and transfer in the soil-rice system. *Chemosphere* 222:314–322
- Shan D, Deng S, Zhao T, Wang B, Wang Y, Huang J, Yu G, Winglee J, Wiesner MR (2016) Preparation of ultrafine magnetic biochar and activated carbon for pharmaceutical adsorption and subsequent degradation by ball milling. *J Hazard Mater* 305:156–163
- Shi T-Z, Feng Y-L, Peng T, Yuan B-G (2021) Sea urchin-shaped Fe₂O₃ coupled with 2D MXene nanosheets as negative electrode for high-performance asymmetric supercapacitors. *Electrochim Acta* 381:138245
- Solis RR, Dinc O, Fang GD, Nadagouda MN, Dionysiou DD (2021) Activation of inorganic peroxides with magnetic graphene for the removal of antibiotics from wastewater, environmental science. *NANO* 8:960–977
- Soran M-L, Opriş O, Lung I, Kacso I, Porav AS, Stan M (2017) The efficiency of the multi-walled carbon nanotubes used for antibiotics removal from wastewaters generated by animal farms. *Environ Sci Pollut Res* 24:16396–16406
- Tan IAW, Ahmad AL, Hameed BH (2008) Adsorption of basic dye on high-surface-area activated carbon prepared from coconut husk: equilibrium, kinetic and thermodynamic studies. *J Hazard Mater* 154:337–346
- Tan Q, Han K, Zhao W, Li P, Liu Z, Li S, Qu X (2021) Synchronous nesting of hollow FeP nanospheres into three-dimensional porous carbon scaffold via salt-template method for performance-enhanced potassium-ion storage, sustainable. *Energy Fuels* 5:844–854
- Thines KR, Abdullah EC, Mubarak NM, Ruthiraan M (2017) Synthesis of magnetic biochar from agricultural waste biomass to enhancing route for waste water and polymer application: a review. *Renew Sustain Energy Rev* 67:257–276
- Wang F, Yao J, Sun K, Xing BS (2010) Adsorption of dialkyl phthalate esters on carbon nanotubes. *Environ Sci Technol* 44:6985–6991
- Wang B, Jiang Y-S, Li F-Y, Yang D-Y (2017) Preparation of biochar by simultaneous carbonization, magnetization and activation for norfloxacin removal in water. *Biores Technol* 233:159–165
- Wang H, Fang C, Wang Q, Chu Y, Song Y, Chen Y, Xue X (2018) Sorption of tetracycline on biochar derived from rice straw and swine manure. *RSC Adv* 8:16260–16268
- Wang J, Zhang M, Zhou R, Li J, Zhao W, Zhou J (2020) Adsorption characteristics and mechanism of norfloxacin in water by γ-Fe₂O₃@BC. *Water Sci Technol* 82:242–254

- Wang Q, Yang M, Qi X, Wang J, Sun K, Li Z, Deng G (2021a) A novel graphene oxide decorated with halloysite nanotubes (HNTs/GO) composite used for the removal of levofloxacin and ciprofloxacin in a wide pH range. *New J Chem* 45:18315–18326
- Wang X-X, Meng Z-F, Liu X, Wang T, Hu X-L, Sun X-X (2021b) Adsorption of BS-18 amphoterically modified bentonite to tetracycline and norfloxacin combined pollutants. *Environ Sci* 42:2334–2342
- Wu S, Hu YH (2021) A comprehensive review on catalysts for electrocatalytic and photoelectrocatalytic degradation of antibiotics. *Chem Eng J* 409:127739
- Wu C, Shi L, Xue S, Li W, Jiang X, Rajendran M, Qian Z (2019) Effect of sulfur-iron modified biochar on the available cadmium and bacterial community structure in contaminated soils. *Sci Total Environ* 647:1158–1168
- Xia Y, Yang T, Zhu N, Li D, Chen Z, Lang Q, Liu Z, Jiao W (2019) Enhanced adsorption of Pb(II) onto modified hydrochar: modeling and mechanism analysis. *Biores Technol* 288:121593
- Xu W-C, Zhong L-B, Shao Z-D, Dou S, Yu L, Cheng X, Zheng Y-M (2021) Rational design of pore structure for carbon aerogels to significantly increase adsorption of tetracycline from water using batch and fixed-bed operation. *Environ Sci Nano*. <https://doi.org/10.1039/D1EN00459J>
- Yang X, Zhang X, Wang Z, Li S, Zhao J, Liang G, Xie X (2019) Mechanistic insights into removal of norfloxacin from water using different natural iron ore – biochar composites: more rich free radicals derived from natural pyrite-biochar composites than hematite-biochar composites. *Appl Catal B Environ* 255:117752
- Yang S, Xue X, Zhang J, Liu X, Dai C, Xu Q, Lian J, Zhao Y, Li G, Li H, Yuan S (2020) Molten salt “boiling” synthesis of surface decorated bimetallic-nitrogen doped carbon hollow nanospheres: An oxygen reduction catalyst with dense active sites and high stability. *Chem Eng J* 395:125064
- Yap MW, Mubarak NM, Sahu JN, Abdullah EC (2017) Microwave induced synthesis of magnetic biochar from agricultural biomass for removal of lead and cadmium from wastewater. *J Ind Eng Chem* 45:287–295
- Zhang Q-Q, Ying G-G, Pan C-G, Liu Y-S, Zhao J-L (2015) Comprehensive evaluation of antibiotics emission and fate in the river basins of China: source analysis, multimedia modeling, and linkage to bacterial resistance. *Environ Sci Technol* 49:6772–6782
- Zhang D, Yang Z, Yang Y, Li H, Wang X (2020) Highly active hollow mesoporous NiFeCr hydroxide as an electrode material for the oxygen evolution reaction and a redox capacitor. *Chem Commun* 56:15549–15552
- Zhou YY, Liu XC, Tang L, Zhang FF, Zeng GM, Peng XQ, Luo L, Deng YC, Pang Y, Zhang JC (2017) Insight into highly efficient co-removal of p-nitrophenol and lead by nitrogen-functionalized magnetic ordered mesoporous carbon: Performance and modeling. *J Hazard Mater* 333:80–87
- Zhou J, Zhang S, Zhou YN, Tang W, Yang J, Peng C, Guo Z (2021a) Biomass-derived carbon materials for high-performance supercapacitors: current status and perspective. *Electrochem Energy Rev* 4:219–248
- Zhou C, Li X, Jiang H, Ding Y, He G, Guo J, Chu Z, Yu G (2021b) Pulverizing Fe₂O₃ Nanoparticles for Developing Fe₃C/NCodoped carbon nanoboxes with multiple polysulfide anchoring and converting activity in Li-S batteries. *Adv Func Mater* 31:2011249